ADVANCED FUNCTIONAL MATERIALS
www.afm-journal.de

Structure and Disorder in Squaraine–C_{60} Organic Solar Cells: A Theoretical Description of Molecular Packing and Electronic Coupling at the Donor–Acceptor Interface

Yao-Tsung Fu, Demetrio A. da Silva Filho, Gjergji Sini, Abdullah M. Asiri, Saadullah Gary Aziz, Chad Risko, and Jean-Luc Brédas**

Organic solar cells based on the combination of squaraine dyes (as electron donors) and fullerenes (as electron acceptors) have recently garnered much attention. Here, molecular dynamics simulations are carried out to investigate the evolution of a squaraine–C_{60} bilayer interface as a function of the orientation and order of the underlying squaraine layer. Electronic couplings between the main electronic states involved in exciton dissociation and charge (polaron pair) recombination are derived for donor–acceptor complexes extracted from the simulations. The results of the combined molecular-dynamics–quantum-mechanics approach provide insight into how the degree of molecular order and the dynamics at the interface impact the key processes involved in the photovoltaic effect.

1. Introduction

The potential for low-cost and large-area solar-energy harvesting has made organic photovoltaics (OPV) a technology of great promise.[1–6] Recent efforts have pushed OPV closer to commercial viability as power conversion efficiencies (PCE) over 9% have been realized in single-junction devices,[7] while 12% PCE has been achieved in multi-junction cells.[8] Much of this development has been due to improvements in terms of materials design, processing procedures, and new device architectures.[9–20] Although these results are encouraging, there remains limited comprehensive understanding of the factors impacting the underlying physical processes that take place in OPV, and in particular how the myriad morphologies available in the active layer influence the final PCEs.

Large absorption coefficients, especially in the red and near-infrared spectral regions, and the ability to tune the solid-state molecular packing have led to recent interest in the use of squaraine dyes as the primary absorbing and hole-transport (electron-donor) material in organic solar cells.[18,21–27] For instance, Thompson, Forrest, and co-workers have exploited 2,4-bis[4-(*N,N*-diphenylamino)-2,6-dihydroxyphenyl] squaraine, DPSQ, see **Figure 1**, as it has good absorption in the red portion of the visible spectrum (>650 nm), while thermal and solvent-vapor annealing (SVA) techniques can be used to manipulate the relative crystallinity/order of DPSQ-C_{60} active layers.[21,23,28] In particular, fine control of the bulk and interfacial morphologies of DPSQ-C_{60} bilayers lead to a 30% increase in PCE (3.4% to 4.8%).[23] The results of these studies, in conjunction with the theoretical underpinnings discussed by Giebink and co-workers,[29,30] suggest that an optimized bilayer OPV should maintain considerable order within the bulk to minimize cell resistance and improve exciton diffusion efficiency while the heterojunction with the acceptor should be rough/disordered to limit the intermolecular electronic coupling (i.e., molecular orbital overlap) between the donor and acceptor to reduce geminate charge (polaron-pair) recombination.[23] In addition, Würthner and co-workers reported on the aggregation-dependent photovoltaic properties of squaraine-$PC_{61}BM$ (phenyl-C_{61}-butyric acid methyl ester) bulk heterojunctions with both H- and J-aggregates in the mixture;[31] the formation of J-aggregates, which red-shift the absorption maximum, results in increased device efficiency.

Since morphological variability is seen to impact significantly the electronic processes within the bulk and interfacial regions of the active layer,[32–40] it is important to develop insight into the materials behavior at the molecular level. However, it remains very difficult to obtain precise, molecular-scale experimental details concerning the nature of the molecular

Dr. Y.-T. Fu, Prof. D. A. da Silva Filho, Dr. G. Sini, Dr. C. Risko, Prof. J.-L. Brédas
School of Chemistry and Biochemistry and Center for Organic Photonics and Electronics
Georgia Institute of Technology
Atlanta, Georgia 30332-0400, USA
E-mail: chad.risko@chemistry.gatech.edu; jean-luc.bredas@chemistry.gatech.edu
Prof. D. A. da Silva Filho
Universidade de Brasilia
Instituto de Física
Brasilia, DF 70919-970, Brazil
Dr. G. Sini
Laboratoire de Physicochimie des Polymères et des Interfaces (LPPI)
Université de Cergy-Pontoise
5 Mail Gay-Lussac, F-95031, Cergy-Pontoise Cedex, France
Prof. A. M. Asiri, Prof. S. G. Aziz, Prof. J.-L. Brédas
Department of Chemistry
Faculty of Science
King Abdulaziz University
Jeddah 21589, Saudi Arabia

DOI: 10.1002/adfm.201303941

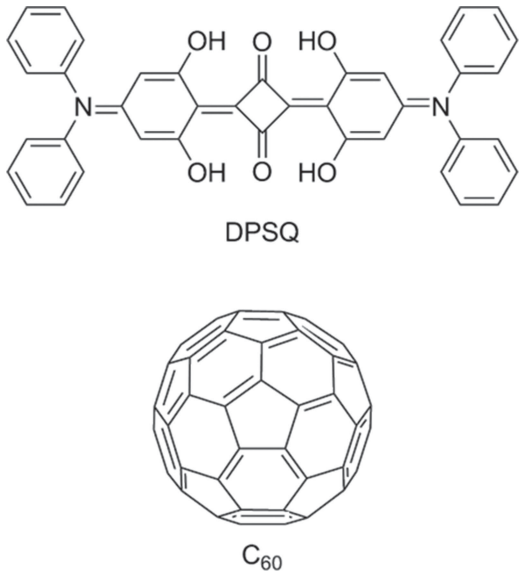

Figure 1. Chemical structures of the donor 2,4-bis[4-(*N*,*N*-diphenylamino)-2,6-dihydroxyphenyl] squaraine (DPSQ) and the acceptor C_{60}.

packing configurations in these regions,[29,30,41] in particular in the presence of disorder. It is the reason why molecular dynamics (MD) simulations are increasingly used as a tool to gain further understanding of the bulk and interfacial morphologies[35,42–45] with recent results highlighting the potential for intermixing and/or disorder at bilayer interfaces. Here, our goal is to employ MD simulations to investigate the bilayer squaraine–C_{60} interface morphology and couple them with electronic-structure calculations to analyze how the electronic properties evolve as a function of interfacial configurations (see Computational Methods for full details). A key finding is that the combination of molecular shape, local packing configurations, and dynamics lead to relatively small electronic couplings among the interfacial electronic states of importance in the photovoltaic process at squaraine-C_{60} interfaces.

2. Results and Discussion

Our discussion is structured as follows. We first describe the key features of the DPSQ slabs that are used to examine interfacial molecular packing morphologies available as a function of the processing methods outlined previously.[23] We then examine the strength of the intermolecular interactions expected between C_{60} and DPSQ as a function of DPSQ orientation, and use the DPSQ slabs to examine the nature of the DPSQ-C_{60} interface. Finally, we analyze how the nature and dynamics of these interfaces influence the intermolecular donor-acceptor electronic couplings.

2.1. Ordered and Disordered DPSQ Slabs

Controlling the degree of order of DPSQ in the bulk and at the interface is an important factor that impacts the PCE of the DPSQ-C_{60} bilayer OPV. As a first step, we examine two slab configurations that correspond to films developed through differing processing procedures described previously:[23] an ordered configuration (O) to represent more crystalline films, and a disordered configuration (D) to represent the as-cast, amorphous DPSQ film:

i) Ordered: Both thermal and solvent-vapor annealing procedures prior to C_{60} deposition (denoted as 'Pre-C_{60}') lead experimentally to an ordered, crystalline DPSQ film with a molecular d-spacing of 15 Å.[22] Notably, this d-spacing differs from that found in solvent-grown crystals of DPSQ[22] and is shorter than the full length of an isolated DPSQ molecule (≈19 Å) determined from the molecular geometry in the solvent-grown crystal. Here, we use two crystal facets—the (001) and (1-11) surfaces (see **Figure 2**)—to represent ordered structures as the exact nature and orientation of the ordered DPSQ film are not experimentally known.
ii) Disordered: As-cast DPSQ films show no observable order.[23] For both the (001) and (1-11) slabs, a series of annealing simulations over a range of temperatures (T = 300 K to 800 K) were undertaken to create a representative set of amorphous/disordered films prior to interaction with C_{60}.

To characterize the packing of the DPSQ molecules in the slabs, it is useful to define two angles that allow an easy description of the molecular orientations (see **Figure 3**): firstly ϕ, the angle between the squaraine short axis (defined as the axis connecting the oxygen atoms of the squaraine core) and the substrate surface (*xy* plane in Figure 3). If $\phi = 0°$, the short axis is parallel ('flat') with the surface, while for $\phi = 90°$, the short axis is perpendicular to the surface. This axis proves to

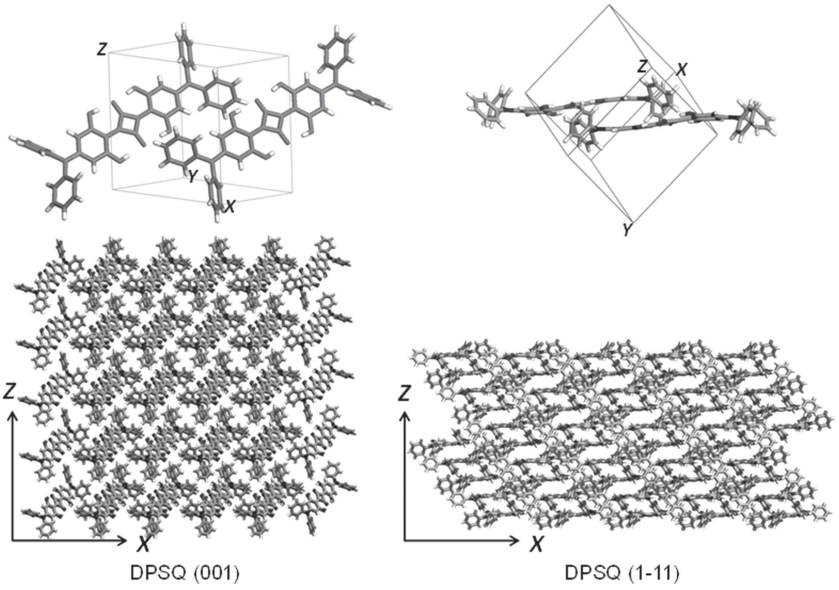

Figure 2. Depictions of the DPSQ (001) and (1-11) surfaces.The two top panels represent the cleavage (*xz*) planes.

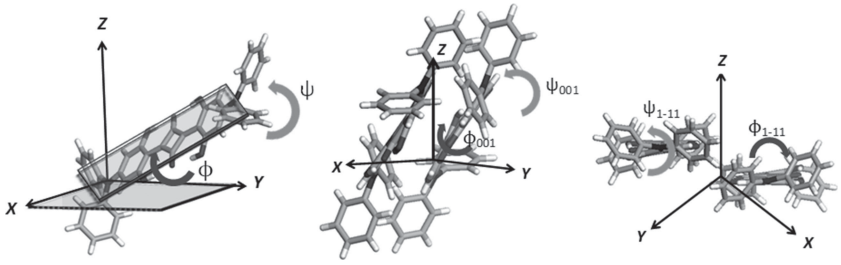

Figure 3. [left] Illustration of the orientation angles between the squaraine short axis (ϕ) and long axis (ψ) and the slab face (xy plane). Representations of ϕ and ψ for [middle] the (001) slab and [right] the (1–11) slab. See text for further detail.

be a critical factor to describe the relative packing geometries of the DPSQ molecules at the interface; secondly ψ, the angle between the squaraine long axis (defined as the axis connecting the nitrogen atoms) and the substrate surface (xy plane in Figure 3). If $\psi = 0°$, the long axis is parallel ('flat') with the surface, while for $\psi = 90°$, the long axis is perpendicular to the surface. There is minimal change (≈5°) to ψ for both (001) and (1-11) slabs on going from the bulk to the slab. The same is true for the (001) slab even after interaction with C_{60}. For the (1-11) slab, however, there is a larger disruption to ψ after interaction with C_{60} (see the Supporting Information, SI, for further details).

According to the above definitions, the angles are $\phi_{001} = 53°$ and $\psi_{001} = 51°$ for the (001) slabs and $\phi_{1\text{-}11} = 0°$ and $\psi_{1\text{-}11} = 4.5°$ for the (1-11) slabs. Based on the ψ angles, it is seen that the DPSQ molecules have a mostly 'upright' orientation at the (001) surface and a 'flat' orientation at the (1-11) surface.

To examine the impact of temperature on order within the DPSQ phase and to create amorphous DPSQ slabs, the crystalline (001) and (1-11) slabs were annealed over a broad temperature range (T= 300 K to 800 K). As shown by the orientation probability distribution in **Figure 4**, both the (001) and (1-11) surfaces remain relatively stable from 300 K to 340 K, with the orientation distributions becoming broader and shifting slightly with increasing temperature. At temperatures over 400 K, ϕ_{001} shows a large shift to a more perpendicular orientation (from 53° to 75°), while $\phi_{1\text{-}11}$ has a more modest shift (from 10° to 22°) and remains relatively flat. On the other hand, both ψ_{001} and $\psi_{1\text{-}11}$ reorient only slightly (see the SI for further details). We note that the thermally-modified orientations are maintained on cooling and do not revert to the original crystalline orientation (as anticipated given the simulation time and procedure).

When temperatures reach above 600 K, however, significant reorientations/rearrangements occur. This is evidenced through evaluation of the nematic order parameter (S), based on the cosine of the angle (θ) determined between the director vector of all DPSQ molecules and the orientational vector of each individual DPSQ molecule. S is defined as:[46]

$$S = \langle P_2(\cos\theta)\rangle = \left\langle \frac{3}{2}\cos^2\theta - \frac{1}{2} \right\rangle \quad (1)$$

where $P_2(x)$ is a second-order Legendre polynomial. The orientational vector for each DPSQ molecule is determined by the long axis of the squaraine backbones; the director vector is the overall direction of preferred molecular orientation of the DPSQ molecules. The order parameter for all DPSQ molecules was computed separately and averaged. By definition, S = 0 means the molecular orientation is isotropic, while increasing S reveals higher order; as a point of reference, typical order parameters for liquid crystals can range between 0.4 and 0.9 as a function of temperature.[47] **Figure 5** depicts the order parameters of the (001) and (1-11) slabs as a function of annealing temperature. The (001) and (1-11) slabs maintain a relatively good degree of order until ≈630–670 K. Annealing at temperatures >700 K removes any order and an amorphous-like structure appears. These high-temperature structures, then, are used as the basis for simulations involving disordered slabs.

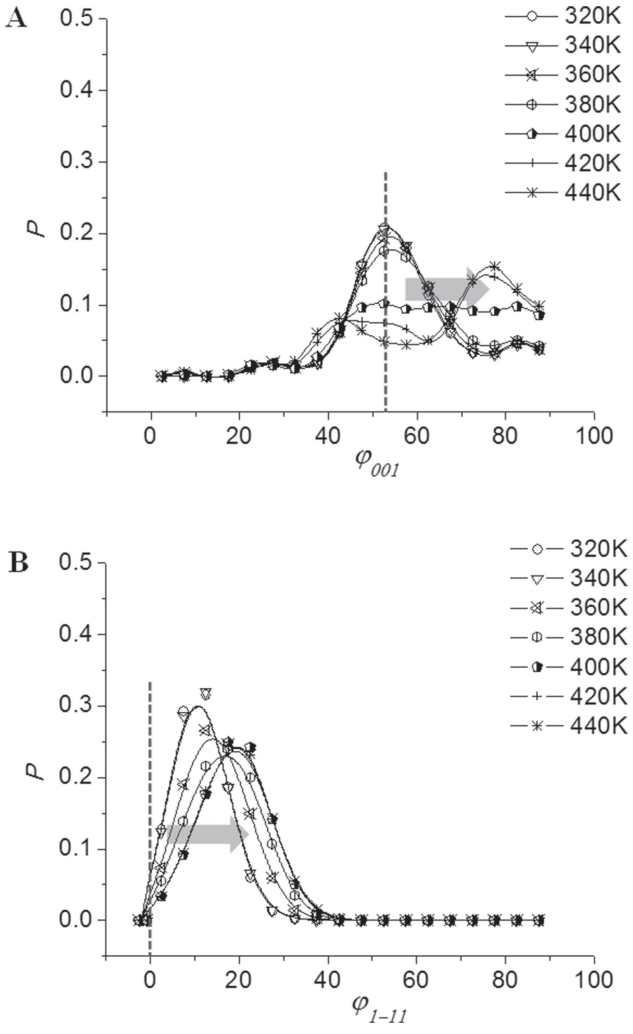

Figure 4. Orientation probability distributions (P) for ϕ for (A) the (001) slabs and (B) the (1-11) slabs as a function of temperature. The dotted lines show the orientations in the experimental X-ray structures, while the arrows show the general orientation shifts with increasing temperature.

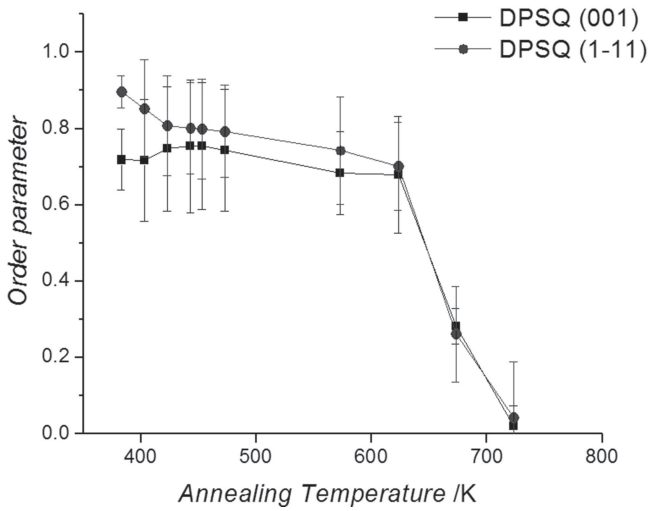

Figure 5. Nematic order parameters for the DPSQ (001) and (1-11) slabs as a function of annealing temperature.

2.2. Squaraine-C_{60} Complex and Surface Interactions

The (001) and (1-11) surfaces present two different DPSQ long-axis orientations with respect to the surface, mostly upright (ψ_{001}) and flat ($\psi_{1\text{-}11}$); hence, different interactions between the DPSQ molecules and C_{60} can be expected. For the upright orientation of (001), the fullerenes are susceptible to interact more strongly with the periphery phenyl rings, while the flat orientation of (1-11) opens the squaraine core up to contact with the fullerene.

As a preliminary step in our investigation of the squaraine–C_{60} interface, we evaluated the binding energy of a single DPSQ–C_{60} complex via molecular mechanics energy minimization. As expected, a face-on configuration of the DPSQ–C_{60} complex (representative of the (1-11)–C_{60} interface) is significantly more strongly bound than an edge-on (mainly phenyl-fullerene) interaction (–12.5 kcal/mol compared to –6.6 kcal/mol, respectively; see Figure S14 in the SI). However, it is important to note that, on the DPSQ surface, the three-dimensional molecular shape of DPSQ (due to the orientation of the periphery phenyl rings), the orientations of the DPSQ short and long axes, and the off-set DPSQ packing arrangements that lead to the corrugated nature of the slab surfaces, do not directly allow for such idealized face-on or edge-on donor-acceptor packing configurations. However, evaluations of the cohesive energies for the interaction of a single C_{60} on the (1-11) surface (–60.1 ± 5 kcal/mol) versus the (001) surface (–36.6 ± 2 kcal/mol), see **Figure 6**, are consistent with the results for the isolated-complex binding energies.

2.3. The Squaraine–C_{60}Interface: Impact of the Squaraine Order

To derive a picture of how a C_{60} layer develops on DPSQ, a series of MD simulations were run at 300 K for the DPSQ slabs described above with $n \cdot C_{60}$ molecules, where n = 1, 3, 5, 10, 15, 20, 25, 30, 130; these values allow for C_{60} coverages that range from sub-monolayer (n < 32) up to ~four molecular layers

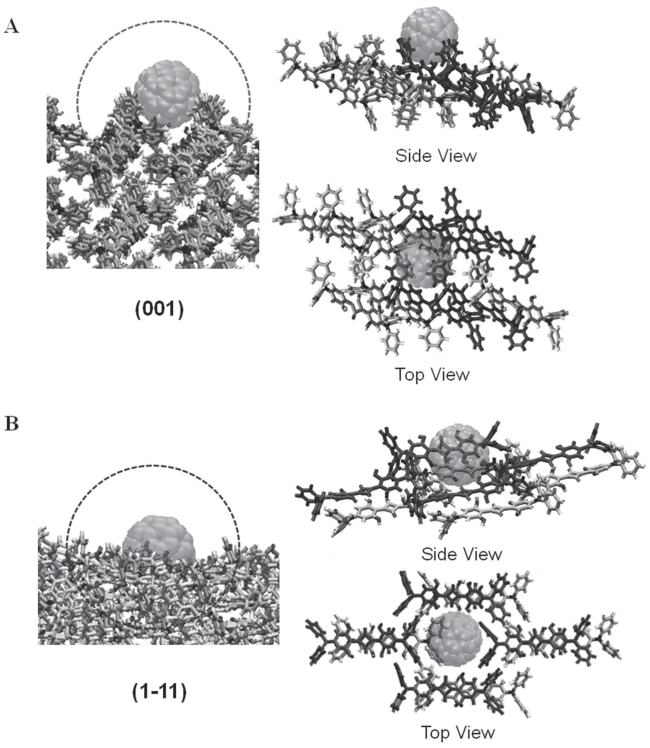

Figure 6. Side and top views of the interaction of a single C_{60} on: (A) the (001) surface; and (B) the (1-11) surface at 300 K. The circles on the left correspond to the zoomed-in areas depicted on the right, where the darker DPSQ molecules represent those directly adjacent to C_{60}.

(n = 130) of C_{60} (see **Figure 7**). We start the discussion with the ordered DPSQ films at low surface coverage (n = 1–10). In the case of the (001) surface, the C_{60} molecules tend to fill the empty channels formed around the outer phenyl groups of the DPSQ molecules (Figures 6A and 7A). As the coverage increases, the C_{60} molecules fully occupy these channels and then start to fill in the areas directly above the phenyl groups. There is little evidence of intermixing among the DPSQ cores and the C_{60} molecules, as can be seen by the positioning of the DPSQ centers-of-mass (COM) in Figure 7C (see SI for further details). However, the orientation distribution of ϕ_{001} does broaden and shift to a peak value of 85°, that is, orientations similar to those found upon thermal annealing of the surface (see above). In our simulations, no regular packing configuration of the fullerene molecules on the surface (such as fcc or hcp) are observed, which is related to the corrugated nature of the (001) surface. This is different from what was obtained upon deposition of fullerenes on the (001) surface of pentacene (where the long axis of the pentacene are nearly perpendicular to the surface plane); in that instance, the C_{60} molecules are found to arrange in an hcp fashion.[42] While our results for the DPSQ (001)–C_{60} interface contrast with the proposed templating effect of ordered DPSQ films,[23] we note that the C_{60} film thicknesses considered here are very thin and that the timescale of our simulations does not allow for crystallization to occur.

We now turn to the (1-11) surface. At low C_{60} surface coverage (n = 1–10), the fullerenes either settle into the 'holes'

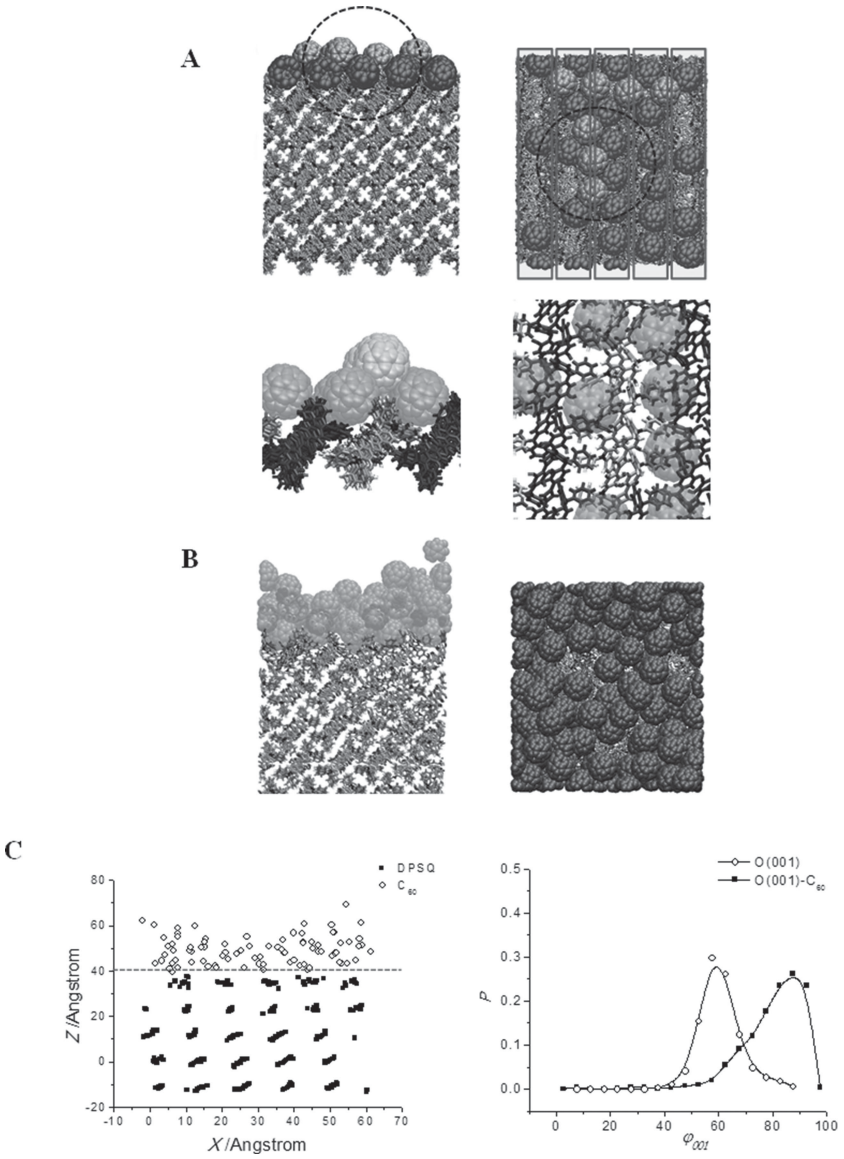

Figure 7. Side [left] and top [right] views of the DPSQ (001)-C_{60} interface after a 1.2 ns simulation with (A) 30 and (B) 130 C_{60} molecules; close and far-field views are provided for clarity. The transparent boxes [top-right in 7A] highlight the channels formed by the outer phenyl groups, while the darker molecules simply provide contrast among different DPSQ molecules; the circles represent the area for which the close-field images are displayed. (C) [left] Center-of-mass distribution for the (001) slab upon deposition of 130 C_{60} molecules; the dotted line represents the position of the original interface; [right] orientation probability distributions (P) for ϕ in the case of the (001) DPSQ slab with and without C_{60} at 300 K.

(**Figure 8**) formed on the DPSQ surface or pack on top of the π-backbone of the squaraines. As the surface coverage increases, the C_{60} molecules tend to move more deeply into the holes and assemble into clusters, causing a displacement of the DPSQ molecules in the upper layers. This can be seen from: (i) the orientation distribution, as the distribution broadens considerably with respect to that for the slab prior to interaction with C_{60}; and (ii) the mixing of the DPSQ and C_{60} molecules at the interface, as manifested by an analysis of the centers of mass in Figure 8C (see SI for further details). We note that similar results related to intermixing were observed for C_{60} deposited on the pentacene (010) surface (for which the pentacene backbones are parallel to the surface).[42] Overall, the results of our molecular dynamics simulations reveal major differences between the (001) and (1-11) slabs in terms of the available local morphologies, and are consistent with expectations coming from the results discussed above in terms of the interaction and cohesive energies.

Finally, we have considered interfaces starting from the completely disordered DPSQ slabs created by high-temperature annealing; we also examined how further annealing, within the timescales of the simulations, might influence the interface after C_{60} deposition (see **Figure 9**). As expected, the degree of disorder at the interface increases with annealing temperature, leading to more pronounced DPSQ and C_{60} mixing as observed through analysis of the center-of-mass distributions for DPSQ and C_{60} (see SI). The orientation distributions for these DPSQ slabs are very broad and show no specific orientation, with nematic order parameters less than 0.1. Due to the timescale limitation of our simulations, it is not possible to observe the formation of higher order for either DPSQ or C_{60} as a function of annealing; this contrasts with the observations of Zimmerman and co-workers[23] who showed experimentally that solvent annealing following C_{60} deposition leads to increased order in the C_{60} layer (as evidenced by X-ray diffraction measurements) and some increased order of the (as-cast) disordered DPSQ layer (shown by changes to the UV-vis absorption spectrum which indicate increased aggregation).

2.4. Electronic Couplings as a Function of the Nature of the Interface

The results of the MD simulations underline that the nature of the underlying surface has a profound impact on the interfacial interactions, in terms of the relative molecular orientations and order and the potential for intermixing. We now examine how the electronic couplings between DPSQ and C_{60} molecules depend on the degree of order of the interface morphology and the dynamics of the system at 300 K. We recall that the electronic couplings among the relevant electronic states are critical factors in the charge-recombination and exciton-dissociation processes when cast in the framework of Marcus theory of electron-transfer reaction. To assess these couplings, snapshots from the MD simulations (after thermalization) were collected after every 5 ps of simulation and the coordinates of molecular complexes formed by one DPSQ and one C_{60} molecule in close proximity were

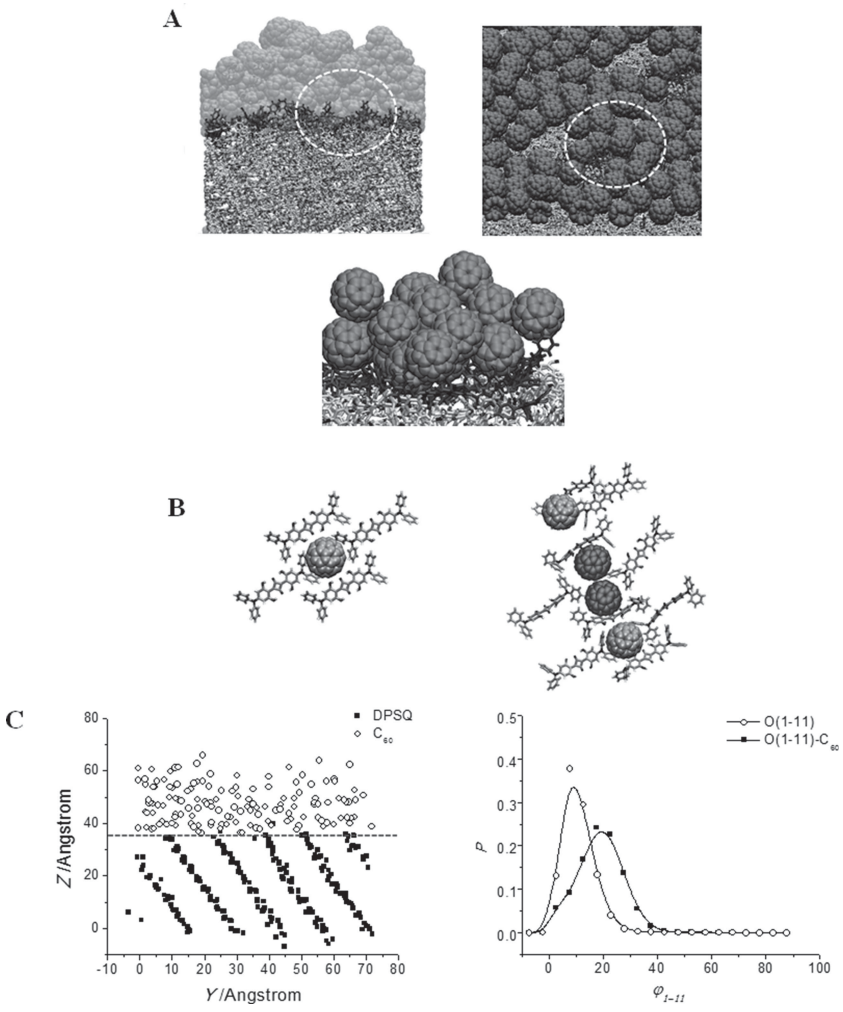

Figure 8. (A) Side and top views of the C_{60}–DPSQ (1-11) interface after a 1.2 ns simulation of the DPSQ (1-11)–C_{60} interface with 160 C_{60} molecules. The darker molecules simply provide contrast among different DPSQ molecules, while the white circle is the area from which the close-field image was captured. (B) Illustration of the "holes" on the (1-11) surface and how C_{60} can infiltrate them. (C) [left] Center-of-mass distribution for the (001) slab upon deposition of 130 C_{60} molecules; the dotted line represents the position of the original interface; [right] orientation probability distributions (P) for ϕ in the case of the (001) DPSQ slab with and without C_{60} at 300 K.

extracted in order to provide relevant geometries for the electronic-coupling calculations. We note that the complexes were chosen at random and that no further geometry optimizations via electronic-structure methods were considered.

The description of exciton-dissociation and charge-recombination pathways requires the evaluation of the intermolecular electronic couplings between, on the one hand, the "local" excited states (e.g., S_1 of the [isolated] donor and acceptor molecules) or the ground state (e.g., S_0 for the donor and acceptor molecules) and, on the other hand, the lowest-lying charge-transfer (CT) state of the donor-acceptor complex. It is useful to bear in mind that C_{60} belongs to the icosahedral (I_h) point group and that the three lowest excited states ($^1T_{1g}$, $^1T_{2g}$, and ^1G_g) are nearly degenerate. In the case of model complexes comprised of C_{60} and pentacene,[39] the contribution of these three states were found to be very similar and as a result it could be safely assumed that the S_1 state arises solely from one of the three terms; we observe similar trends here and thus will only present one of these three couplings without any loss of generality. The electronic couplings were computed for: (i) the ground state (V_{eff}^{SO}) versus the lowest CT state, to examine charge (polaron pair) recombination; and (ii) the local, lowest-excited singlet states on C_{60} (V_{eff}^{SA1}) or DPSQ (V_{eff}^{SD1}) versus the lowest CT state, to examine exciton-dissociation processes. These couplings were evaluated for three DPSQ–C_{60} interfaces at 300 K [involving the (001), (1-11), and disordered DPSQ slabs] as well as two interfaces at 383 K [involving the (001) and (1–11) slabs] to relate to the annealed samples in the literature.[23]

A total of 2400 configurations were used to compute the average (avg), standard deviation (sd), and maximum (max) values for the electronic couplings. A representative histogram of these couplings for the DPSQ (001)–C_{60} interface is shown in **Figure 10** and the full results are summarized in **Table 1**. In general, it is found that the average couplings are very small, on the order of 10 meV or less; however, the maximum values of the electronic couplings, obtained for just a few configurations, can be quite large and are comparable to those obtained for an analogous, idealized ZnPc–C_{60} complex.[48] These results can be understood through examination of the DPSQ frontier molecular orbitals (see Figure S15 in the SI). The DPSQ HOMO and LUMO are located mainly on the DPSQ backbone, with very little weight on the outer phenyl rings (mesomeric effects are expected to be small); in fact, the phenyl rings, which provide significant three-dimensional character to the molecular structure, act to sterically hinder close contact between C_{60} and the central portion of DPSQ where the frontier orbitals reside. Hence, there is a limited number of configurations available that can provide significant electronic couplings.

Considering the results for V_{eff}^{SO}, which describe the coupling parameter of importance for charge recombination between the lowest-lying CT state and the ground state, we observe that both

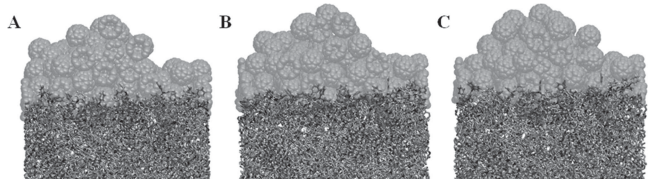

Figure 9. Side-view snapshots of the DPSQ–C_{60}interface starting with an amorphous DSPQ layer. The snapshots are for simulations run at (A) 300 K, (B) 383 K, and (C) 443 K after C_{60} deposition.

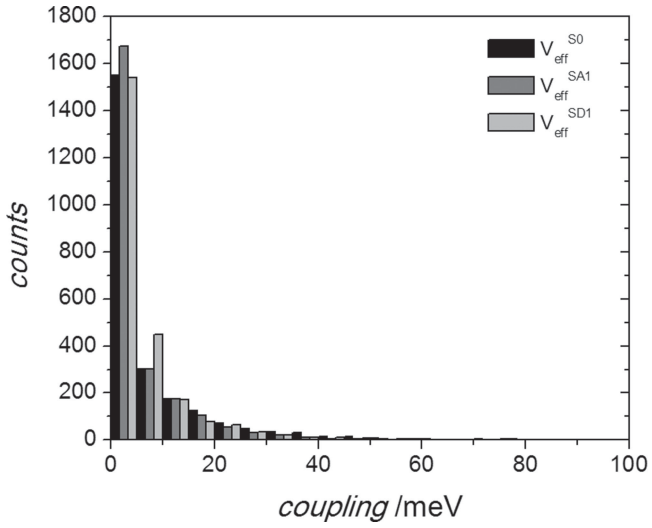

Figure 10. Histogram for the electronic couplings in DPSQ–C_{60} complexes for the (001)–C_{60} interface.

the average and maximum electronic couplings at the (001)–C_{60} and (1–11)–C_{60} interfaces are quite similar, while the maximum values for the amorphous, more disordered interface are substantially smaller. That the (001)–C_{60} and (1-11)-C_{60} interfaces provide such similar couplings might, at first sight, seem contradictory, given the DPSQ orientations described above for these interfaces. However, the combination of: (i) the configurations available for large couplings being in general limited; (ii) the thermal motions of the molecules at 300 K (and 383 K) being rather substantial; and (iii) the degree of disorder (as compared to the amorphous structure) remaining relatively modest, contributes to make the two interfaces behave in a similar fashion in terms of electronic couplings. These results, contrasting the two more ordered interfaces with the amorphous interface, are consistent with the notion put forth by Zimmerman and co-workers that controlling the order and packing at the interface can impact the rates for charge-recombination in this bilayer system.[23]

In terms of V_{eff}^{SA1} and V_{eff}^{SD1}, the couplings of importance to describe the rate for exciton dissociation in a complex, again

Table 1. Average (avg), standard deviation (sd), and maximum (max) values of the electronic couplings between either the ground state (V_{eff}^{SO}) or the lowest local excited singlet states on C_{60} (V_{eff}^{SA1}) or DPSQ (V_{eff}^{SD1}), and the lowest-lying CT state, as a function of interfacial structure and simulation temperature.

Surface	V_{eff}^{SO} [meV]		V_{eff}^{SA1} [meV]		V_{eff}^{SD1} [meV]	
	avg ± sd	max	avg ± sd	max	avg ± sd	max
300 K						
(001)–C_{60}	7 ± 11	116	5 ± 9	80	6 ± 9	103
(1-11)–C_{60}	8 ± 12	127	6 ± 9	95	8 ± 12	151
Amorphous	6 ± 9	65	5 ± 7	60	9 ± 11	122
383 K						
(001)–C_{60}	8 ± 12	82	6 ± 10	97	7 ± 12	139
(1-11)–C_{60}	7 ± 10	121	5 ± 7	75	8 ± 13	167

no clear picture emerges when comparing the different interfaces. However, for all cases, both the maximum and average values of V_{eff}^{SD1} are larger than V_{eff}^{SA1}, pointing to the fact that the exciton dissociation originating from excitation on DPSQ is more efficient than exciton dissociation originating from C_{60} excitation, a trend previously observed for the ZnPc-C_{60} interface.[48]

3. Conclusions

We have performed a series of MD simulations to investigate molecular packing at DPSQ–C_{60} bilayer interfaces as a function of DPSQ orientation and order, as well as electronic-structure calculations to evaluate the electronic couplings between donor and acceptor complexes extracted from the simulation of these interfaces. The presence of the outer phenyl groups on the DPSQ molecules, the corrugation of the ordered surfaces, the impact of disorder arising from thermal annealing and/or interactions with C_{60}, and the overall system dynamics, are seen to lead to very small average electronic couplings (on the order of 10 meV or less) among the electronic states expected to play key roles in the exciton-dissociation or charge-recombination processes.

While the consideration of simple donor-acceptor complexes to describe the electronic processes at the interface provides an admittedly limited picture, important messages still arise concerning the order and dynamics in these systems. In agreement with the postulate of Zimmerman and co-workers,[23] the relative degrees of order/disorder at the interface can impact the electronic couplings responsible for charge-carrier (polaron pair) recombination, though they also influence the electronic couplings for the exciton-dissociation process. However, the most important aspect is that these interfaces are very dynamic, even at 300 K, which reveals a more complex picture for the electronic couplings than the one that would be assumed based on static (i.e., frozen, ideal geometry) models of the interfaces. While the interactions between electron motion and intramolecular as well as intermolecular vibrations have been investigated in great detail in the case of charge-carrier transport, an essential message of the present work is that these interactions are just as important when considering the exciton-dissociation and charge-recombination processes at donor–acceptor interfaces.

4. Computational Methods

All MD simulations were performed with the LAMMPS[49] software package using a modified OPLS-AA (Optimized Potentials for Liquid Simulations – All Atom)[50] force field. Partial charges for DPSQ were determined by a fit of the electrostatic potential obtained from a density functional theory (DFT)-based geometry optimization at the B3LYP/6-31G(d,p) level of theory with Gaussian 09 (Revision B.01).[51]

To develop DPSQ slab models for the interface studies, the crystal structure of Wang and co-workers[22] was used to construct 5 × 5 × 5 (5.6 nm × 5.9 nm × 6 nm, 19 000 atoms) super-cells of the DPSQ (001) and (1–11) lattice (Figure 2). The super-cell periodicity was maintained in the *xy* plane

while a 20-nm void space was created in the *z*-direction to create an isolated slab. For the DPSQ-C_{60} bilayer simulations, the bottom layers of the DPSQ super cell (one layer for the (001) surface and three layers for the (1-11) surface) were constrained to represent interactions with a bulk-like manifold. To investigate how C_{60} interacts and packs on the DPSQ slabs, MD simulations with nC_{60} molecules (n = 1, 3, 5, 10, 15, 20, 25, 30, 130) on the DPSQ slabs were run at 300 K; the C_{60} layer formation ranges from less than one-molecular layer (n < 32) up to four layers (n = 130).

The MD simulations were carried out under the NVT ensemble using the Verlet integrator with a time step of 1 fs; the temperature for equilibration/data collection and annealing was maintained by the Nose-Hoover thermostat. A spherical cutoff of 1.2 nm for the summation of van der Waals interactions and the particle-particle-particle-mesh (PPPM) solver for long-range Coulomb interactions was used throughout. Details concerning: (i) the modified OPLS-AA parameters and force-field validation (including comparisons of select molecular geometric parameters and crystal unit-cell parameters); (ii) the bare (001) and (1-11) surfaces; and (iii) the impact of fixing the bottom-most layers on the molecular packing, are provided in the SI.

To understand the impact of local (donor–acceptor) molecular packing configurations on the electron couplings among a variety of interfacial electronic states, DPSQ–C_{60} complexes were extracted directly from the MD simulations for use in subsequent quantum-mechanics calculations. The electronic couplings for exciton dissociation and charge recombination were computed using a diabatic state approach developed by Coropceanu and co-workers that is based on an INDO/SCI description of the excitonic and charge-transfer electronic wave functions.[39,40,48,52] In the framework of perturbation theory (Fermi Golden Rule), the rates for charge separation and recombination between diabatic states i and f can be expressed as:

$$k_{if} = \left(V_{if}^{eff}\right)^2 \sqrt{\frac{\pi}{\lambda k_B T \hbar^2}} \exp\left[-\frac{\left(\Delta G^0 + \lambda\right)^2}{4\lambda k_B T}\right] \quad (2)$$

where k_B and $\hbar$ are the Boltzmann and Planck constants, respectively; T is the temperature (set to 300 K in our calculations); λ denotes the reorganization energy; V_{if}^{eff} is the effective electronic coupling between the initial and final states; and ΔG^o represents the Gibbs free energy of the electron-transfer reaction. Here, we focus on examinations of the electronic couplings V_{if}^{eff}, evaluated at the INDO[53] level of theory with the Mataga-Nishimoto potential to describe the Coulomb repulsion term,[54,55] as a guide to gain insight into the interplay of molecular structure, order, and dynamics on the electronic processes taking place at the interface.

Supporting Information

Supporting Information is available from the Wiley Online Library or from the author.

Acknowledgements

The work at Georgia Tech was partly supported by the Office of Naval Research (N00014-11-1-0211) and by the Deanship of Scientific Research (DSR), King Abdulaziz University, Jeddah, Saudi Arabia, under Grant No. 23-3-1432/HiCi. We acknowledge with thanks the DSR technical and financial support. D.A.S.F. gratefully thanks the financial support from the Brazilian Research Council's CAPES, CNPq, and FAP-DF. We thank Casey Campbell for initial electronic-structure calculations on DPSQ.

Received: November 22, 2013
Revised: January 10, 2014
Published online: February 27, 2014

[1] B. Kippelen, J. L. Bredas, *Energy Environ. Sci.* **2009**, *2*, 251.
[2] G. Li, R. Zhu, Y. Yang, *Nat. Photon.* **2012**, *6*, 153.
[3] M. A. Green, K. Emery, Y. Hishikawa, W. Warta, E. D. Dunlop, *Prog. Photovolt.: Res. Appl.* **2012**, *20*, 606.
[4] T. Ameri, P. Khoram, J. Min, C. J. Brabec, *Adv. Mater.* **2013**, *25*, 4245.
[5] S. B. Darling, F. You, *RSC Adv.* **2013**, *3*, 17633.
[6] S. R. Forrest, *Nature* **2004**, *428*, 911.
[7] M. A. Green, K. Emery, Y. Hishikawa, W. Warta, E. D. Dunlop, *Prog. Photovolt.: Res. Appl.* **2012**, *20*, 12.
[8] Press release: Heliatek GmbH. January 16, 2013.
[9] C. J. Brabec, J. R. Durrant, *MRS Bull.* **2008**, *33*, 670.
[10] M. Helgesen, R. Sondergaard, F. C. Krebs, *J. Mater. Chem.* **2010**, *20*, 36.
[11] F. C. Krebs, *Sol. Energ. Mat. Sol. C.* **2009**, *93*, 394.
[12] G. Li, V. Shrotriya, J. Huang, Y. Yao, T. Moriarty, K. Emery, Y. Yang, *Nat. Mater.* **2005**, *4*, 864.
[13] X. Yang, J. Loos, S. C. Veenstra, W. J. H. Verhees, M. M. Wienk, J. M. Kroon, M. A. J. Michels, R. A. J. Janssen, *Nano Lett.* **2005**, *5*, 579.
[14] Y. Kim, S. Cook, S. M. Tuladhar, S. A. Choulis, J. Nelson, J. R. Durrant, D. D. C. Bradley, M. Giles, I. McCulloch, C.-S. Ha, M. Ree, *Nat. Mater.* **2006**, *5*, 197.
[15] G. Li, Y. Yao, H. Yang, V. Shrotriya, G. Yang, Y. Yang, *Adv. Funct. Mater.* **2007**, *17*, 1636.
[16] J. Peet, J. Y. Kim, N. E. Coates, W. L. Ma, D. Moses, A. J. Heeger, G. C. Bazan, *Nat. Mater.* **2007**, *6*, 497.
[17] J. T. Rogers, K. Schmidt, M. F. Toney, E. J. Kramer, G. C. Bazan, *Adv. Mater.* **2011**, *23*, 2284.
[18] B. E. Lassiter, J. D. Zimmerman, A. Panda, X. Xiao, S. R. Forrest, *Appl. Phys. Lett.* **2012**, *101*, 063303
[19] S. D. Spencer, C. Bougher, P. J. Heaphy, V. M. Murcia, C. P. Gallivan, A. Monfette, J. D. Andersen, J. A. Cody, B. R. Conrad, C. J. Collison, *Sol. Energ. Mat. Sol. C.* **2013**, *112*, 202.
[20] Y. Zhou, C. Fuentes-Hernandez, J. Shim, J. Meyer, A. J. Giordano, H. Li, P. Winget, T. Papadopoulos, H. Cheun, J. Kim, M. Fenoll, A. Dindar, W. Haske, E. Najafabadi, T. M. Khan, H. Sojoudi, S. Barlow, S. Graham, J.-L. Brédas, S. R. Marder, A. Kahn, B. Kippelen, *Science* **2012**, *336*, 327.
[21] N. N. Wang, J. D. Zimmerman, X. R. Tong, X. Xiao, J. S. Yu, S. R. Forrest, *Appl. Phys. Lett.* **2012**, *101*, 133901.
[22] S. Y. Wang, L. Hall, V. V. Diev, R. Haiges, G. D. Wei, X. Xiao, P. I. Djurovich, S. R. Forrest, M. E. Thompson, *Chem. Mater.* **2011**, *23*, 4789.
[23] J. D. Zimmerman, X. Xiao, C. K. Renshaw, S. Y. Wang, V. V. Diev, M. E. Thompson, S. R. Forrest, *Nano Lett.* **2012**, *12*, 4366.
[24] D. Bagnis, L. Beverina, H. Huang, F. Silvestri, Y. Yao, H. Yan, G. A. Pagani, T. J. Marks, A. Facchetti, *J. Am. Chem. Soc.* **2010**, *132*, 4074.
[25] L. Beverina, M. Crippa, M. Landenna, R. Ruffo, P. Salice, F. Silvestri, S. Versari, A. Villa, L. Ciaffoni, E. Collini, C. Ferrante, S. Bradamante, C. M. Mari, R. Bozio, G. A. Pagani, *J. Am. Chem. Soc.* **2008**, *130*, 1894.

[26] U. Mayerhöffer, K. Deing, K. Gruß, H. Braunschweig, K. Meerholz, F. Würthner, *Angew. Chem. Int. Ed.* **2009**, *48*, 8776.
[27] G. D. Wei, X. Xiao, S. Y. Wang, K. Sun, K. J. Bergemann, M. E. Thompson, S. R. Forrest, *ACS Nano* **2012**, *6*, 972.
[28] J. D. Zimmerman, B. E. Lassiter, X. Xiao, K. Sun, A. Dolocan, R. Gearba, D. A. Vanden Bout, K. J. Stevenson, P. Wickramasinghe, M. E. Thompson, S. R. Forrest, *ACS Nano* **2013**, *7*, 9268.
[29] N. C. Giebink, G. P. Wiederrecht, M. R. Wasielewski, S. R. Forrest, *Phys. Rev. B* **2010**, *82*, 155305.
[30] N. C. Giebink, B. E. Lassiter, G. P. Wiederrecht, M. R. Wasielewski, S. R. Forrest, *Phys. Rev. B* **2010**, *82*, 155306.
[31] K. C. Deing, U. Mayerhoffer, F. Wurthner, K. Meerholz, *Phys. Chem. Chem. Phys.* **2012**, *14*, 8328.
[32] H. Yamagata, J. Norton, E. Hontz, Y. Olivier, D. Beljonne, J. L. Bredas, R. J. Silbey, F. C. Spano, *J. Chem. Phys.* **2011**, *134*, 204703.
[33] T. M. Clarke, J. R. Durrant, *Chem. Rev.* **2010**, *110*, 6736.
[34] M. Linares, D. Beljonne, J. Cornil, K. Lancaster, J. L. Bredas, S. Verlaak, A. Mityashin, P. Heremans, A. Fuchs, C. Lennartz, J. Ide, R. Mereau, P. Aurel, L. Ducasse, F. Castet, *J. Phys. Chem. C* **2010**, *114*, 3215.
[35] T. Liu, D. L. Cheung, A. Troisi, *Phys. Chem. Chem. Phys.* **2011**, *13*, 21461.
[36] D. P. McMahon, D. L. Cheung, A. Troisi, *J. Phys. Chem. Lett.* **2011**, *2*, 2737.
[37] A. Ojala, A. Petersen, A. Fuchs, R. Lovrincic, C. Pölking, J. Trollmann, J. Hwang, C. Lennartz, H. Reichelt, H. W. Höffken, A. Pucci, P. Erk, T. Kirchartz, F. Würthner, *Adv. Funct. Mater.* **2012**, *22*, 86.
[38] S. Verlaak, D. Beljonne, D. Cheyns, C. Rolin, M. Linares, F. Castet, J. Cornil, P. Heremans, *Adv. Funct. Mater.* **2009**, *19*, 3809.
[39] Y. Yi, V. Coropceanu, J. L. Bredas, *J. Am. Chem. Soc.* **2009**, *131*, 15777.
[40] Y. Yi, V. Coropceanu, J. L. Bredas, *J. Mater. Chem.* **2011**, *21*, 1479.
[41] B. A. Collins, J. E. Cochran, H. Yan, E. Gann, C. Hub, R. Fink, C. Wang, T. Schuettfort, C. R. McNeill, M. L. Chabinyc, H. Ade, *Nat. Mater.* **2012**, *11*, 536.
[42] Y. T. Fu, C. Risko, J. L. Bredas, *Adv. Mater.* **2013**, *25*, 878.
[43] L. Muccioli, G. D'Avino, C. Zannoni, *Adv. Mater.* **2011**, *23*, 4532.
[44] R. A. Cantrell, C. James, P. Clancy, *Langmuir* **2011**, *27*, 9944.
[45] N. R. Tummala, S. Mehraeen, Y.-T. Fu, C. Risko, J.-L. Brédas, *Adv. Funct. Mater.* **2013**, *23*, 5800.
[46] M. R. Wilson, *J. Mol. Liq.* **1996**, *68*, 23.
[47] C. McBride, C. Vega, L. G. MacDowell, *Phys. Rev. E* **2001**, *64*, 011703.
[48] B. P. Rand, D. Cheyns, K. Vasseur, N. C. Giebink, S. Mothy, Y. P. Yi, V. Coropceanu, D. Beljonne, J. Cornil, J. L. Bredas, J. Genoe, *Adv. Funct. Mater.* **2012**, *22*, 2987.
[49] S. Plimpton, *J. Comput. Phys.* **1995**, *117*, 1.
[50] W. L. Jorgensen, J. Tirado-Rives, *J. Am. Chem. Soc.* **1988**, *110*, 1657.
[51] M. J. Frisch, G. W. Trucks, H. B. Schlegel, G. E. Scuseria, M. A. Robb, J. R. Cheeseman, G. Scalmani, V. Barone, B. Mennucci, G. A. Petersson, H. Nakatsuji, M. Caricato, X. Li, H. P. Hratchian, A. F. Izmaylov, J. Bloino, G. Zheng, J. L. Sonnenberg, M. Hada, M. Ehara, K. Toyota, R. Fukuda, J. Hasegawa, M. Ishida, T. Nakajima, Y. Honda, O. Kitao, H. Nakai, T. Vreven, J. A. Montgomery Jr., J. E. Peralta, F. Ogliaro, M. Bearpark, J. J. Heyd, E. Brothers, K. N. Kudin, V. N. Staroverov, T. Keith, R. Kobayashi, J. Normand, K. Raghavachari, A. Rendell, J. C. Burant, S. S. Iyengar, J. Tomasi, M. Cossi, N. Rega, J. M. Millam, M. Klene, J. E. Knox, J. B. Cross, V. Bakken, C. Adamo, J. Jaramillo, R. Gomperts, R. E. Stratmann, O. Yazyev, A. J. Austin, R. Cammi, C. Pomelli, J. W. Ochterski, R. L. Martin, K. Morokuma, V. G. Zakrzewski, G. A. Voth, P. Salvador, J. J. Dannenberg, S. Dapprich, A. D. Daniels, O. Farkas, J. B. Foresman, J. V. Ortiz, J. Cioslowski, D. J. Fox, Gaussian Inc., Wallingford, CT **2010**.
[52] T. Kawatsu, V. Coropceanu, A. J. Ye, J. L. Bredas, *J. Phys. Chem. C* **2008**, *112*, 3429.
[53] J. Ridley, M. Zerner, *Theoret. Chim. Acta* **1973**, *32*, 111.
[54] N. Mataga, K. Nishimoto, *Z. Phys. Chem.* **1957**, *12*, 335.
[55] N. Mataga, K. Nishimoto, *Z. Phys. Chem.* **1957**, *13*, 140.